15th International Symposium on Particle Image Velocimetry – ISPIV 2023
June 19–21, 2023, San Diego, California, USA

Characterization of Binder Drop-Powder Interactions in Binder-Jetting 3D Printing

Zachary Pakulniewicz and Yang Liu[1*]

[1] City College of New York, Department of Mechanical Engineering, New York, NY, USA

∗ Corresponding authors: yliu7@ccny.cuny.edu

Abstract

Binder jetting additive manufacturing (AM) is an innovative form of 3D printing that generates complex and advanced structures of various materials by jetting binder drops onto a powder bed. The drops on the bed cure the powder to form structures in a quick and efficient manner. However, the method suffers several flaws, including manufacturing inconsistencies and coarse resolution of structures. These flaws are essentially caused by the complex interactions between the binder drop and the powder during the printing process. Therefore, a better understanding of these interactions will be instrumental in the development of binder jetting for fabricating multipurpose, higher quality functional structures. In this study, these complex interactions are analyzed during the impact and subsequent processes. The impact dynamics of binder drops on a powder surface were examined by using a custom impingement rig under various test conditions (i.e., different impact velocities and binder viscosities). A high-speed Random-Dots-Projecting-Imaging (RDPI) system was developed and used to capture the transient details of the drop-powder interactions. It was found that during the binder-jetting 3D printing, a sequence of dynamic stages would occur, including initial contact, spreading, imbibition/drainage, receding (Imbibition), rebounding, and primitive formation.

1 Introduction

Additive manufacturing (AM) has rapidly emerged as one of the most lucrative and promising industrial markets in recent times. This innovative process, often referred to as "3D printing," involves the precise deposition of material in three axes to construct physical structures (Shahrubudin et al. 2019). AM printers utilize a reference CAD file to guide the selective jetting process and fabricate the desired structure. While several AM methods such as stereolithography (SLA), selective laser sintering (SLS), and fused deposition modeling (FDM) have gained prominence in recent years, they often suffer from limited versatility (Lee et al. 2017). These commonly used AM techniques are restricted by a lack of material variety and the inability to print at room temperature and standard atmospheric pressure (Oropallo and Piegl 2016). Therefore, there is a growing demand for new technologies that can overcome these limitations and operate under such conditions. Binder jetting AM presents itself as a potential solution to address these constraints. By employing this technique, a wider range of materials can be utilized, and printing can be performed at room temperature and standard atmospheric pressure, providing greater versatility in the AM process. Binder jetting AM offers the promise of breaking through the conditional limitations of traditional AM methods, opening up new possibilities for diverse applications and manufacturing capabilities.

Binder jetting AM operates similarly to other AM technologies, where selective jetting is employed to create a structure on a surface. However, unlike other methods, binder jetting involves the deposition of a liquid onto a powder material (Mostafaei et al. 2021). This liquid, known as a binder drop, consists of a

binding agent mixed with DI-water to enhance its viscosity. The selective jetting of binder drops facilitates the adhesion of the material powder on the printing bed, enabling it to take shape according to the desired design (Mostafaei et al. 2021). As the process advances, a fresh layer of powder is rolled over the bed using a piston. Subsequently, the desired material solidifies, resulting in a consolidated product.

Unfortunately, binder jetting technology still has some unresolved manufacturing flaws. Structures produced through binder jetting often exhibit lower relative density and higher surface porosity, primarily stemming from the use of powdered materials (Mostafaei et al. 2021). As a result, additional post-processing steps, such as densification or curing, are typically required to address these issues (Gibson et al. 2021). However, it is important to note that these post-processing steps can introduce challenges, including potential distortion of the structure geometry and reduced mechanical properties compared to structures manufactured using techniques like SLS. Therefore, further research and development efforts are necessary to overcome these limitations associated with binder jetting.

These limitations are due to various factors. One theory suggests that extrinsic properties of the powder, such as porosity, contribute to the nonuniform and variable impact of binder drops (Mostafaei et al. 2021). These interactions may involve the tunneling and cratering of binder drops into the powder, resulting in geometric variations. Additionally, the impact of a binder drop on a powder bed leads to the ejection of powder particles, creating pores beneath the surface (Parab et al. 2019; Barui et al. 2020). A better understanding of the micro-physical details during the impact of the binder drops and the interactions between the binder drop and powder is strongly desired to mitigate these flaws during the printing process.

Over the past years, while many studies have been conducted to investigate the dynamic processes during drop-powder interactions, most of them have relied on either high-speed imaging (Bai et al. 2019; Pakulniewicz and Liu 2023) or X-ray imaging (Parab et al. 2019; Barui et al. 2020) technologies, in which only the in-plane changes of the impacting drop and the powder particle movements at the selected slices can be recorded qualitatively. As a result, the intricate details of the evolutionary behavior of binder drops impacting on a powder bed and the complex interactions between the dynamically evolving binder drop and the powder bed surface remain largely unexplored due to the lack of knowledge about the transient surface morphological details during the dynamic courses of the printing process. Advanced experimental techniques, which are capable of making time-resolved, quantitative measurements of the powder surface morphologies during the printing processes, are highly desirable to provide a more comprehensive understanding of the intricate dynamics taking place at the powder surface during the binder-jetting 3D printing process.

In the present study, we introduce a novel optical-based 3D scanning method known as the high-speed random-dots-projection-imaging (RDPI) technique. This innovative technique enables us to perform quantitative and temporally-resolved full-field measurements of the powder surface morphologies during drop-powder interactions. This will provide a better understanding of the underlying mechanisms governing binder drop-powder interactions. In the subsequent sections, we will first describe the experimental methods employed in this study. These methods enable us to capture detailed information about the powder surface morphologies during the interaction with binder drops. Through quantitative measurements of the powder surface morphologies, we can analyze both the temporal evolution and spatial variation of the binder-jetted powder surfaces.

2 Materials and Methods

2.1 Binder and Powder Materials

Although binder research is a novelty topic, there have been numerous studies that have prompted the discussion on binder-powder interactions. The following materials were inspired by the work of Rajniak, et al (Rajniak et al. 2007) in the research to determine the effect of binder properties on the morphology of the powder bed. Binder solutions (2%, 5%, 10% w/w) of hydroxypropyl-cellulose (HPC) were prepared by gently stirring HPC-SL (Nisso Soda Co. Ltd., Tokyo, Japan) into deionized water at a constant rate. The stirring occurred overnight to allow proper degassing and hydration of the solution. Higher concentration of HPC mixed in deionized water results in a higher viscosity of binder. Binder properties were extrapolated from data provided from the Nisso Soda Co. Ltd. Website and given in Table 1.

Table 1: Binder viscosity at specified concentrations.

*Viscosity (mPa*s)*	*Concentration (%)*
7.00	2.0
40.0	5.0
85.0	8.0
200.0	10.0

Dimensionless values of binder drops are useful for predicting the printability of a drop (de Ruijter et al. 1999). Supplemental data such as dynamic viscosity μ and surface tension γ were found through data provided by the Nisso Soda Co. Ltd. website as well as the previous study performed by Rajniak (Rajniak et al. 2007). The Reynolds number is defined in Equation 1:

$$Re = \frac{\rho dV}{\mu} \tag{1}$$

where ρ is the density of the binder fluid, d is the binder drop diameter, and V is the drop impact velocity. The Weber number is defined in Equation 2:

$$We = \frac{\rho dV^2}{\gamma} \tag{2}$$

The relationship between the Reynolds and Weber number are particularly valuable for determining drop printability. Through a reciprocation of the Ohnesorge number formula as given in Equation 3:

$$\frac{1}{Oh} = \frac{Re}{\sqrt{We}} \tag{3}$$

When the reciprocal of the Ohnesorge number is between 1 and 14, binder drops are observed to experience good jettability (Guo et al. 2017). Table 2 documents these values for each of the tested binder drops, listed by viscosities of HPC.

Table 2: Binder viscosity with respective printability

Viscosity (Pa·s)	*1/Ohnesorge*
0.0122	18.98
0.0195	11.08
0.165	1.20

Although each concentration experiences different velocities by case and thereby different Reynolds and Weber numbers by case, the relationship between them (i.e., the reciprocal of the Ohnesorge number) remains constant. The powder used to jet the binder drops onto was chosen to be hydroxypropyl-cellulose and has a mean diameter of 90 μm.

2.2 Experimental Setup

A custom impingement rig was constructed for binder drop release under the testing conditions as shown in Fig. 1. The impingement rig is responsible for simulating the binder drop jetting process (Bai et al. 2019) using a needle clamp stand, a 22-gauge needle, and a syringe pump (New Age NE-300).

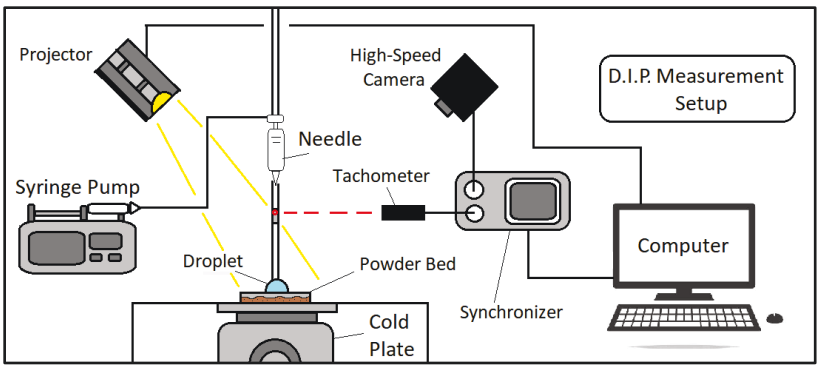

Figure 1: A schematic of the experimental setup used in the present study.

The syringe pump is connected via tubing to a glass syringe filled with binder solution, where it is consequently jetted onto the powder bed. This process is captured simultaneously by a high-speed imaging system and an RDPI system to investigate the interactions between the binder and powder upon impact. The height of the needle is adjusted to allow different impact velocities to be created. In the present study, three impact velocities are tested: 1.51m/s, 2.10m/s, and 2.59m/s.

A high-speed RDPI system was implemented to capture the transient details of the complex binder-powder interactions. The high-speed imaging system consists of the high-speed camera (Photron FastCam WX-100), a high-resolution projector system, a laser trigger system (tachometer) to trigger the camera and projector as the drop passes through, a synchronizer (BNC 575 Series) to connect the two devices, and a computer with the PFV4 software installed to record the images as the camera captured them. All images were captured at 5000fps at a shutter rate of 1/10000s and resolution of 1280 × 512 pixels. The camera is set to center triggering mode during recording to the PFV4 software. Additionally, all images were post-processed in the ImageJ software using contrast adjustment and a background removal algorithm.

3 Random-Dots-Projection-Imaging (RDPI) Technique

The RDPI technique is an upgrade of the digital-image-projection (DIP) technique (Liu et al. 2020a), which relies on actively projecting known light patterns onto an object, and extracting 3D surface shapes from the images of the projected light patterns captured from one or more points of view(Salvi et al. 2010). The correspondence for the RDPI technique is established by finding the displacement vectors between corresponding points in the measured images (i.e., the images with the droplet sitting on the powder surface) and a reference image (i.e., the image of the flat smooth powder surface without droplet). The displacement vectors can be derived by applying a spatial cross-correlation image processing algorithm (similar to the conventional particle image velocimetry(PIV) post-processing algorithm), as shown in Fig. 2. During the RDPI measurements, the random dots images are captured by using a high-speed camera. The instantaneous displacement map of the random dots can be calculated based on every two successive images.

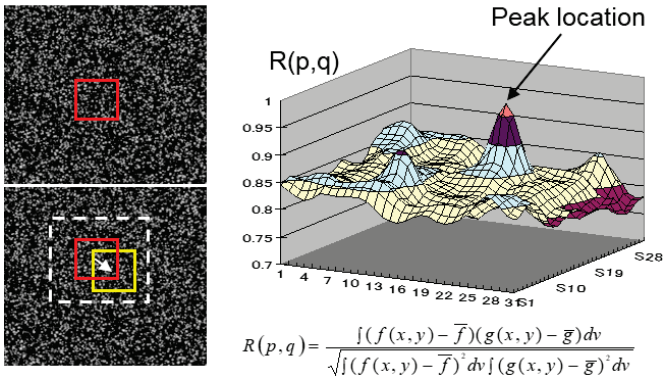

Figure 2. Diagram of 2D cross-correlation to calculate the displacement map in the RDPI technique.

The 3D shape of the measured object is restructured based on the displacement map of the corresponding points between the measured images and the reference image. Figure 3 shows the schematic to illustrate the technical basis of the RDPI technique. A digital projector is used to project random-dots image patterns onto a test object of interest. Due to the 3D nature of the surface shape of the test object, the projected image patterns will deform when observed from a different perspective other than the projection axis. The projection unit, image acquisition unit, and the three-dimensional object form a triangulation base. If the corresponding points between the camera and the projector are identified through a calibration procedure, the 3-D shape of the test object can be obtained through an analysis of the triangulation.

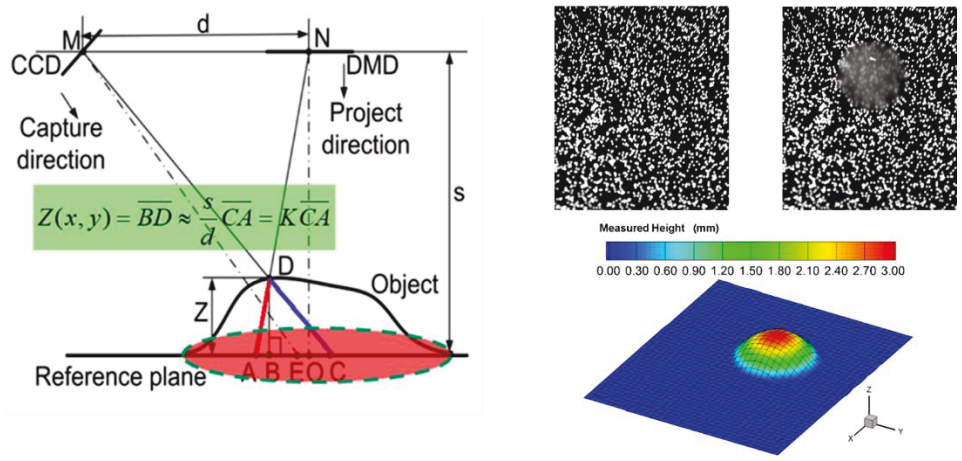

Figure 3. Diagram of the displacement-to-height conversion in the RDPI measurements.

As shown in Fig. 3, a reference plane with a height 0 in the Z-direction is used as the reference surface for all subsequent measurements. The arbitrary point "*M*" in the captured image corresponds to point "*N*" in the projected image, and point "*D*" on the object surface. From the projector's point of view, point "*D*" on the object surface has the same position as point "*A*" on the reference plane. However, from the point of view of the image recording camera, point "*D*" on the object surface images will be at the same position as the point "*C*" on the reference plane. Therefore, the same point "*N*" in the projected image will be recorded as the point "*A*" in the reference image (i.e., the image acquired with the powder surface being flat) and point "*C*" in the distorted image (i.e., the image acquired after the binder drop impacts the surface). The distance between point "*A*" and point "*C*" represents the displacement of the same point "N" between the distorted and reference images. Assume the distance between point "*M*" and point "*N*" is *d*, and the reference plane is parallel to the device with a distance *s* between them. Similar triangles can be formed between ΔMND and ΔCAD, therefore:

$$\frac{d}{\overline{CA}}=\frac{s-\overline{BD}}{\overline{BD}}=\frac{s}{\overline{BD}}-1 \tag{4}$$

Because the distance *s* is usually much larger than $\overline{BD}$, this equation can be simplified as:

$$Z(x,y)=\overline{BD}\approx\frac{s}{d}\overline{CA}=K\overline{CA} \tag{5}$$

It should be noted that, because the values of *s* and *d* are fixed for a given RDPI setup, *K* will be a constant for a given system, which can be determined through a calibration procedure. Equation 4 shows a linear relationship between measured displacement $\overline{CA}$ and the object height *Z(x, y)*. Therefore, the 3D shape of the test object can be determined quantitatively by measuring the displacements between the distorted and reference images at the points of interest.

It should be noted that the correspondence for the RDPI technique used in this study is established by finding the displacement vectors between corresponding points in the distorted images (i.e., the images acquired after the binder drop impacts the powder surface) and a reference image (i.e., the image acquired before the drop impact) by using the spatial cross-correlation image processing algorithm (Zhang et al. 2015; Liu et al. 2020b). This is very different from the most-commonly-used fringe-based structured light technique, in which the 3D profile of the test object with respect to the reference plane is retrieved based on the measured phase changes between the modulated fringe patterns and those in the reference image(Salvi et al. 2010). Figure 3 also shows an example measurement of the 3D profile of a semisphere drop sitting on a flat surface. It can be seen that through the RDPI post processing algorithm, the 3D feature of the semisphere can be well reconstructed. In comparison to the DIP technique, the newly-developed RDPI technique has several advantages: (1) flexibility in camera-projector alignment; (2) controlled dot density to achieve better spatial resolution; and (3) faster image/data processing speed.

4 Results and Discussions

4.1 Transient Surface Morphologies of Powder Surface Interacting with Binder Drop

Figures 4 to 6 show the different dynamic stages of the binder drop impacting a powder surface. Both the raw images and the processed RDPI results are shown in the figures. As can be seen clearly in Fig. 4, when the binder drop impacts the powder surface, a cratering process occurs instantly during the initial contact. Along with the formation of a crater, the binder drop deforms quickly, i.e., spreading, over the powder surface.

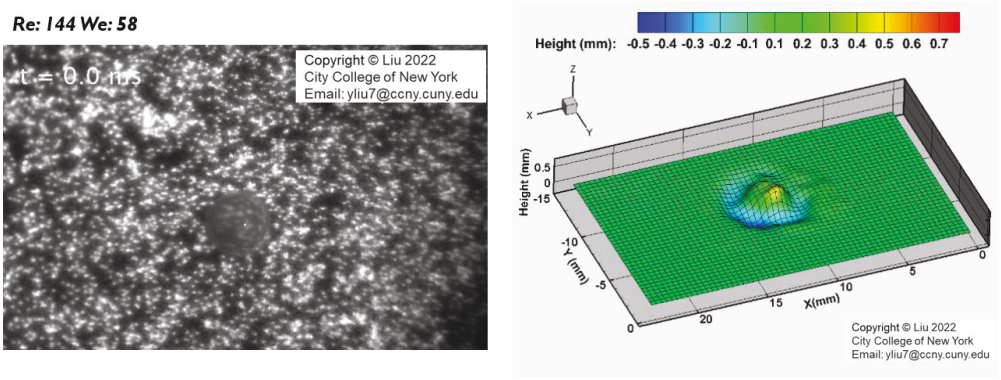

Figure 4: Initial contact of the binder drop on the powder surface.

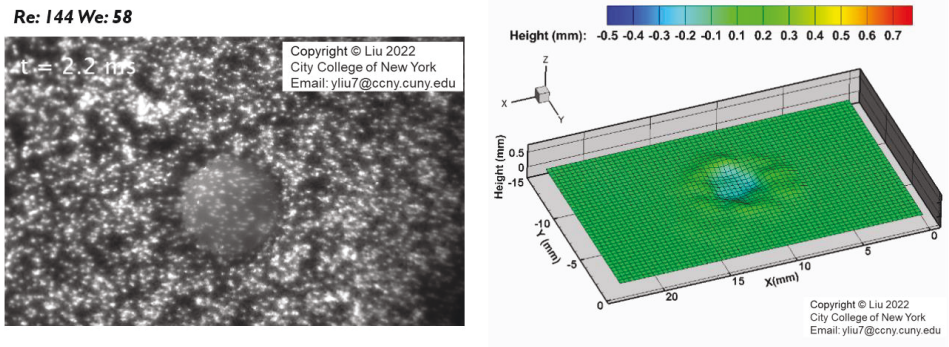

Figure 5: Spreading of the binder drop on the powder surface.

During the spreading process, while some powder particles are absorbed by the binder liquid, the drop expands into a pancake shape, covering the powder surface that is lowered due to the cratering effect, as

shown in Fig. 5. It should be noted that an ejection process of the powder particles is also initiated due to the transfer of kinetic energy from the drop to the powder particles.

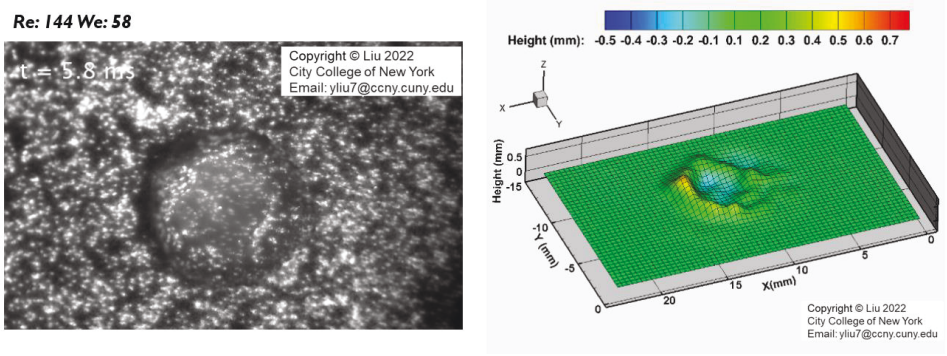

Figure 6: Receding of the binder drop on the powder surface.

After the binder drop spreads to the maximum diameter, due to the surface tension effects, the drop starts to recede over the powder surface as shown in Fig. 6. Along with the receding process, more powder particles are absorbed into the binder liquid, i.e., imbibition. Based on the RDPI data, it is found that the binder drop deepens into the powder with some ridge features formed around the receding drop. It is also observed that the receding binder drop is no longer in a circular shape due to the complex interactions. It should be noted that while the binder drop recedes to smaller areas, the ejected powder particles continue expanding, as clearly shown in Fig. 6.

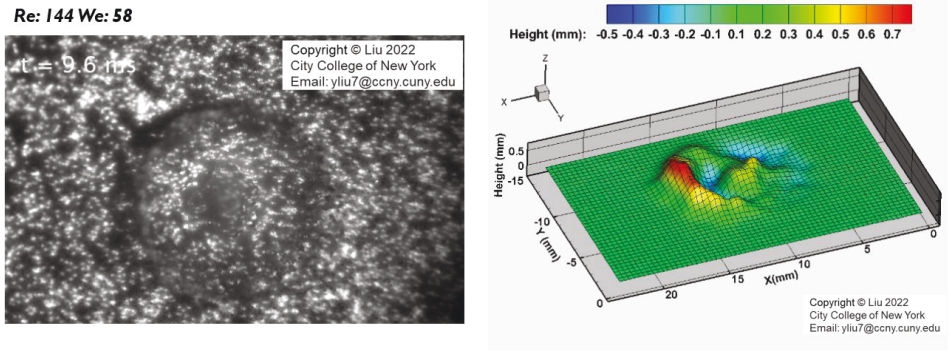

Figure 7: Rebounding of the binder drop on the powder surface.

As the binder drop recedes, it continues to crater into the powder and forms a dense liquid-particle mixture ball, as shown in Fig. 7. Depending on the impact velocity and viscosity of the binder drop, a rebounding process may occur. During the receding and rebounding process, while the binder drop changes in morphology, the ridge features formed on the powder surface during the drop spreading stage are kept in shape as shown in Fig. 7.

4.2 Slice Profiles of Powder Surface during the Dynamic Binder Drop Impacting Process

Based on the results obtained from the RDPI measurements, as depicted in Figures 4 to 7, we can extract height profiles at different time intervals. Figure 8 illustrates the height profiles of a slice along the centerline in the x-direction. It is evident that the height distribution undergoes significant variations during the impacting and deforming processes of the binder drop. Initially, the profile reflects the shape of the binder drop upon impact. However, it is important to note that the initial distribution of pores is non-uniform, leading to drastic and random deformations of the powder surface depending on the location of drop penetration.

In the specific case shown in Figure 8, upon contact between the binder drop and the surface, the powders at X = 13 mm exhibit lower density compared to other locations. Consequently, the drop swiftly penetrates into the powder surface, resulting in a noticeable indentation. Over time, as the binder drop

spreads, the liquid (or liquid/particle mixture) rapidly fills the earlier-formed indentation. Simultaneously, the surface powder particles undergo redistribution throughout this process. These observations highlight the dynamic nature of the binder drop-powder interactions and the complex interplay between the liquid binder and the powder bed. The non-uniformity of the powder surface and the redistribution of particles play a significant role in the overall morphology of the impacted region.

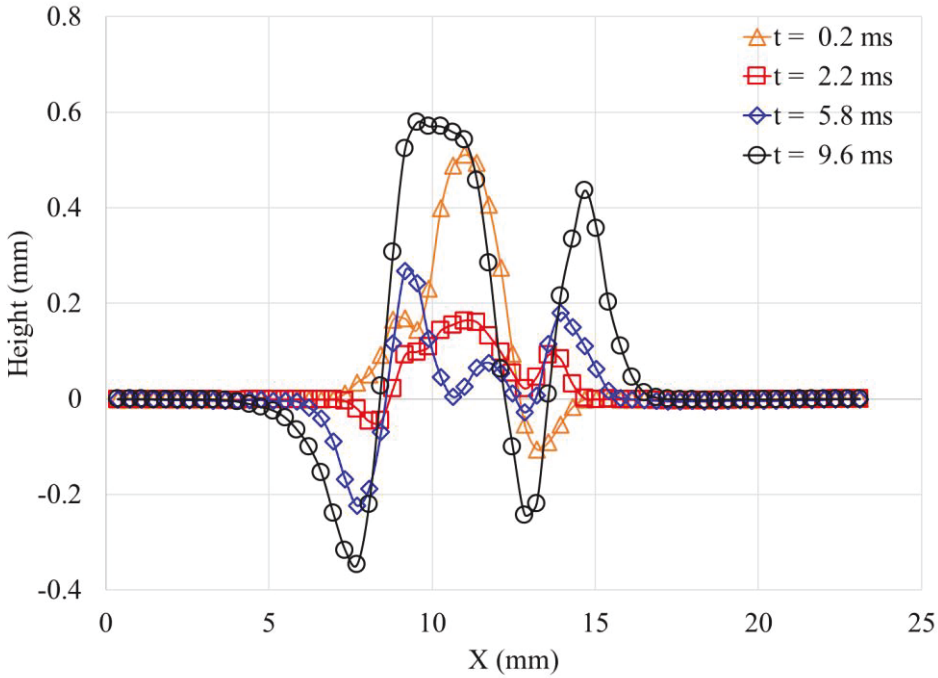

Figure 8: Rebounding of the binder drop on the powder surface.

The redistribution of the powder mass can give rise to the formation of new pores while causing the disappearance of previously formed pores. Consequently, the spreading binder liquid may infiltrate the powder bed unevenly, as depicted at t = 5.8 s in Figure 8. Additionally, it is observed that during the spreading process, numerous powder particles are transported outward, resulting in the formation of ridges at the periphery. Once the binder drop reaches its maximum diameter during spreading, it initiates a recoil motion, which involves the absorption of particles into the binder liquid and further penetration into the powder bed. This behavior is clearly illustrated in Figure 8. As the binder drop recoils back to its minimum diameter, distinctive valley-like features are formed around the binder-particle mixture ball.

These observations highlight the dynamic nature of the binder drop-powder interactions and the complex behaviors exhibited during the spreading and recoiling processes. The redistribution of powder mass, along with the transportation of particles and the formation of valleys and ridges, contribute to the overall morphological changes occurring on the powder surface.

5 Conclusions

In the present study, we experimentally investigated the interactions between binder drops and the powder bed to enhance our fundamental understanding of the dynamic processes involved in binder-jetting additive manufacturing. The experiments were conducted using a custom impingement rig under various test conditions, including different impact velocities and binder viscosities. To capture the transient details of the drop-powder interactions, a novel technique called Random-Dots-Projection-Imaging (RDPI) was developed and implemented.

The application of the RDPI technique proved effective in capturing the dynamics of the binder drops and the powder surface, as well as their transient interactions. Through this technique, a series of dynamic

stages were characterized during the impact of the binder drop on the powder surface. These stages include initial contact, spreading, imbibition/drainage, receding (imbibition), rebounding, and primitive formation.

Furthermore, the RDPI measurements allowed for the extraction of height profiles along any selected slices, enabling a more detailed understanding of the dynamics of binder drop penetration and particle absorption processes. This information contributes to a comprehensive understanding of the dynamic behavior and interaction between binder drops and the powder bed in binder-jetting additive manufacturing. The findings from this study provide valuable insights that can be used to improve the control and optimization of binder-jetting processes, leading to enhanced manufacturing outcomes and the production of high-quality functional structures.

Acknowledgments

The research work is partially supported by the City College of New York via faculty start-up funds. The support of the National Science Foundation (NSF) under award number of CBET-2242311 is also gratefully acknowledged.

References

Bai Y, Wall C, Pham H, et al (2019) Characterizing Binder-Powder Interaction in Binder Jetting Additive Manufacturing Via Sessile Drop Goniometry. Journal of Manufacturing Science and Engineering, Transactions of the ASME 141:. https://doi.org/10.1115/1.4041624/367169

Barui S, Ding H, Wang Z, et al (2020) Probing Ink-Powder Interactions during 3D Binder Jet Printing Using Time-Resolved X-ray Imaging. ACS Appl Mater Interfaces 12:34254–34264. https://doi.org/10.1021/ACSAMI.0C03572/ASSET/IMAGES/LARGE/AM0C03572_0007.JPEG

de Ruijter MJ, de Coninck J, Oshanin G (1999) Droplet spreading: Partial wetting regime revisited. Langmuir 15:2209–2216. https://doi.org/10.1021/LA971301Y/ASSET/IMAGES/LARGE/LA971301YF00005.JPEG

Gibson I, Rosen D, Stucker B, Khorasani M (2021) Binder Jetting. Additive Manufacturing Technologies 237–252. https://doi.org/10.1007/978-3-030-56127-7_8

Guo Y, Patanwala HS, Bognet B, Ma AWK (2017) Inkjet and inkjet-based 3D printing: Connecting fluid properties and printing performance. Rapid Prototyp J 23:562–576. https://doi.org/10.1108/RPJ-05-2016-0076/FULL/PDF

Lee JY, An J, Chua CK (2017) Fundamentals and applications of 3D printing for novel materials. Appl Mater Today 7:120–133. https://doi.org/10.1016/J.APMT.2017.02.004

Liu Y, Jiang X, Lee C, Hu H (2020a) An experimental study on the spatiotemporal evolution of sand waves/ripples in turbulent boundary layer airflow. Physics of Fluids 32:063304. https://doi.org/10.1063/1.5144522

Liu Y, Zhang K, Tian W, Hu H (2020b) An experimental study to characterize the effects of initial ice roughness on the wind-driven water runback over an airfoil surface. International Journal of Multiphase Flow 126:103254. https://doi.org/10.1016/j.ijmultiphaseflow.2020.103254

Mostafaei A, Elliott AM, Barnes JE, et al (2021) Binder jet 3D printing—Process parameters, materials, properties, modeling, and challenges. Prog Mater Sci 119:100707. https://doi.org/10.1016/J.PMATSCI.2020.100707

Oropallo W, Piegl LA (2016) Ten challenges in 3D printing. Eng Comput 32:135–148. https://doi.org/10.1007/S00366-015-0407-0/FIGURES/15

Pakulniewicz Z, Liu Y (2023) An Experimental Study on the Dynamics of Binder Drops Impacting on a Powder Surface in Binder Jetting Additive Manufacturing. In: AIAA SCITECH 2023 Forum. American Institute of Aeronautics and Astronautics

Parab ND, Barnes JE, Zhao C, et al (2019) Real time observation of binder jetting printing process using high-speed X-ray imaging. Scientific Reports 2019 9:1 9:1–10. https://doi.org/10.1038/s41598-019-38862-7

Rajniak P, Mancinelli C, Chern RT, et al (2007) Experimental study of wet granulation in fluidized bed: impact of the binder properties on the granule morphology. Int J Pharm 334:92–102. https://doi.org/10.1016/J.IJPHARM.2006.10.040

Salvi J, Fernandez S, Pribanic T, Llado X (2010) A state of the art in structured light patterns for surface profilometry. Pattern Recognit 43:2666–2680. https://doi.org/10.1016/J.PATCOG.2010.03.004

Shahrubudin N, Lee TC, Ramlan R (2019) An Overview on 3D Printing Technology: Technological, Materials, and Applications. Procedia Manuf 35:1286–1296. https://doi.org/10.1016/J.PROMFG.2019.06.089

Zhang K, Wei T, Hu H (2015) An experimental investigation on the surface water transport process over an airfoil by using a digital image projection technique. Exp Fluids 56:1–16. https://doi.org/10.1007/s00348-015-2046-z